Simultaneous segmentation and distortion correction on diffusion weighted MR using shape priors

Oscar Esteban[1,2], Alessandro Daducci[2], Meritxell Bach-Cuadra[2,3], Jean-Philippe Thiran[2,3], Andrés Santos[1], and Dominique Zosso[2,4]

[1] Biomedical Image Technologies (BIT), ETSI Telecomunicación - Universidad Politécnica de Madrid and CIBER-BBN,
Av. Complutense 30, E-28040 Madrid, Spain
phd@oscaresteban.es,
[2] Signal Processing Laboratory (LTS5), École Polytechnique Fédérale de Lausanne (EPFL)
EPFL STI IEL LTS5, Station 11, CH-1015 Lausanne, Switzerland
[3] Dept. of Radiology, University Hospital Center (CHUV) and University of Lausanne (UNIL)
Rue du Bugnon 46, CH-1011 Lausanne, Switzerland
[4] Department of Mathematics, University of California, Los Angeles (UCLA)
520 Portola Plaza, Box 951555, Los Angeles, CA 90095-1555, USA

Abstract In whole-brain connectivity analysis of diffusion weighted MR images (DWI), an accurate delineation of the white-matter and grey-matter surfaces is required. While high-standard segmentation is readily available for anatomical MRI, such as T1-weighted, DWI typically have drastically lower resolution and severe geometrical distortions. We propose a DWI segmentation-registration framework that exploits the detailed anatomy extracted from anatomical MRI as shape-prior. We use an "active contours without edges"-like model to look for a deformation field that optimally maps the shape prior on the multivariate features in diffusion space. This joint approach reflects the intrinsic coupling of segmentation and distortion correction. Complementary, a precise and consistent cortical parcellation on DWI is straightforward by projection from T1 space. Thus, we expect to improve the reliability and robustness of the resulting connectivity networks and their comparability within and across subjects. First results on synthetic datasets and simulated DWI confirm the effectiveness of our approach.

Keywords: magnetic resonance, diffusion weighted imaging, distortion correction, segmentation, registration, shape priors, connectomics, echo planar imaging

1 Introduction

diffusion weighted imaging (DWI) is a widely used family of magnetic resonance (MR) techniques [31] which recently has accounted for a growing interest in its application to whole-brain structural connectivity analysis. This emerging field, coined in 2005 as *MR Connectomics* [15, 30], currently includes a large amount of imaging techniques for acquisition, processing, and analysis specifically tuned for DWI data.

The whole-brain connectivity analysis has given rise to some challenges towards reliable structural information about the neuronal tracts from DWI [21, 22]. The earlier stages of these processing pipelines generally include two necessary steps, brain

tissue segmentation on the diffusion space and the correction of geometrical distortions inherent to the imaging techniques [16].

In this work, we will refer as brain tissue segmentation to the precise delineation of the cerebrospinal fluid (CSF)-grey matter (GM) and GM-white matter (WM) interface surfaces. This segmentation is an processing step on which strongly rely further tasks. In tractography, a high-standard WM mask is required. Otherwise, there is an important risk for the algorithm to lose fiber bundles. This requirement is usually solved in practice by plainly thresholding the fractional anisotropy (FA), a well-known scalar map derived from DWI which depicts the isotropy of water diffusion inside the brain. A precise location of the GM-WM surface is also essential in the final steps to achieve a consistent parcellisation of the cortex to represent the nodes of the output network. This parcellisation is generally defined in a high-resolution and better understood structural magnetic resonance imaging (MRI) of the same subject (e.g. T1-weighted (T1) and/or T2-weighted (T2) weighted acquisitions). Even though some efforts have addressed the study of the robustness of tractography with respect to intra-subject variability [35, 17], these results are restricted to some regions of the brain, only. Therefore, robust and precise segmentation methods are required in the whole-brain application.

The DWI data is usually obtained with echo-planar imaging (EPI) acquisition techniques, that often suffer from severe distortions due to local field inhomogeneities. Generally, it is appreciated in the anterior part of the brain, along the phase-encoded direction. Some methodologies have been developed and generically named as *EPI-unwarp* techniques [18, 19, 20, 29]. These methods usually require the extra acquisition of the magnitude and phase of the field ("field-mapping"), a condition which is not always met. Some other methodologies do not make use of the field-mapping, compensating the distortion with non-linear registration from structural MRI or other means [1]. To our knowledge, there exists no study on the impact of the EPI distortion on the variability of tractography results.

Therefore, the problems of precise segmentation in DWI-space and the spatial mapping between these contours and the corresponding surfaces in anatomical images bear significant redundancy. Once the spatial relationship between T1 and DWI space is established, the contours which are readily available in T1 space, can simply be projected on to the DWI-data. Conversely, if a precise delineation in DWI-space was achieved, the spatial mapping with T1-space could be derived from one-to-one correspondences on the contours. However, neither segmentation nor registration can be performed flawlessly, if considered independently. The significant benefits of exploiting the anatomical MRI when segmenting the DWI data have been demonstrated [40], justifying the use of the shape prior information.

We suggest clustering the current methodologies of template-based segmentation methods into three groups. The first group typically adds a shape prior term to the energy functional of an evolving active contour [7, 26, 34, 39, 10, 6, 8, 3] These methods generally have a explicit description of the expected relative boundary locations of the object to be delineated, and some even model the statistical deviations from this average shape. Closely related to this group are atlas-based segmentation methods [28, 27, 36, 12, 11], where the prior imposes consistent voxel-based classification of contiguous regions. Here, the presence of more structures than one unique region of

interest (ROI) helps aligning the target image with the atlas in a hierarchical fashion. Finally, the third group generalizes the atlas to actual images, and the contour is to segment simultaneously two different target images, related by a spatial transform to be co-estimated [37, 38].

In this paper we propose a novel registration framework to simultaneously solving the segmentation and distortion challenges, by exploiting as strong shape-prior the detailed anatomy extracted from anatomical MRI. Indeed, hereafter we consider the segmentation in anatomical images as a solved problem. Moreover, the shape prior is of very "strong" nature, since it is specific to the particular subject. Also, after global alignment using existing approaches, the remaining spatial deformation between anatomical and diffusion space is due to MR distortion. Finally, we need to establish precise spatial correspondence between the surfaces in both spaces, including the tangential direction for parcellation. Therefore, we can reduce the problem to finding the differences of spatial distortion in between anatomical and diffusion weighted (DW) space. We thus reformulate the segmentation problem as an inverse problem, where we seek for an underlying deformation field (the distortion) mapping from the structural space into the diffusion space, such that the structural contours segment optimally the DWI data. In the process, the one-to-one correspondence between the contours in both spaces is guaranteed, and projection of parcellisation to DW space is implicit and consistent.

We test our proposed joint segmentation-registration model on two different synthetic examples. The first example is a scalar sulcus model, where the CSF-GM boundary particularly suffers from partial volume effect (PVE) and can only be segmented correctly thanks to the shape prior and its coupling with the inner, GM-WM boundary through the imposed deformation field regularity. The second case deals with more realistic DWI data stemming from phantom simulations of a simplistic brain data. Again, we show that the proposed model successfully segments the DWI data based on two derived scalar features, namely FA and mean diffusivity (MD), while establishing an estimate of the dense distortion field.

The rest of this paper is organized as follows. First, in section 2 we introduce our proposed model for joint multivariate segmentation-registration. Then we provide a more detailed description of the data and experimental setup in section 3. We present results in section 4 and conclude in section 5.

2 Methods

2.1 active contours without edges-like variational segmentation model

Let us denote $\{c_i\}_{i=1..N_c}$ the nodes of a shape prior surface. In our application, a precise WM-GM interface extracted from a high-resolution reference volume. All the formulations can be naturally extended to include more shape priors. On the other hand, we have a number of DWI-derived features at each voxel of the volume. Let us denote by x the voxel and $f(x) = [f_1, f_2, \ldots, f_N]^T(x)$ its associated feature vector.

The transformation from reference into DWI coordinate space is achieved through a dense deformation field $u(x)$, such that:

$$c_i' = T\{c_i\} = c_i + u(c_i) \tag{1}$$

Since the nodes of the anatomical surfaces might lay off-grid, it is required to derive $u(x)$ from a discrete set of parameters $\{u_k\}_{k=1..K}$. Densification is achieved through a set of associated basis functions Ψ_k (e.g. rbf, interpolation splines):

$$u(x) = \sum_k \Psi_k(x) u_k \qquad (2)$$

Consequently, the transformation writes

$$c_i' = T\{c_i\} = c_i + u(c_i) = c_i + \sum_k \Psi_k(c_i) u_k \qquad (3)$$

Based on the current estimate of the distortion u, we can compute "expected samples" within the shape prior projected into the DWI. Thus, we now estimate region descriptors of the DWI features $f(x)$ of the regions defined by the priors in DWI space. Using Gaussian distributions as region descriptors, we propose an active contours without edges (ACWE)-like, piece-wise constant, variational image segmentation model (where the unknown is the deformation field) [5]:

$$E(u) = \sum_{\forall R} \int_{\Omega_R} (f - \mu_R)^T \Sigma_R^{-1} (f - \mu_R) dx \qquad (4)$$

where R indexes the existing regions and the integral domains depend on the deformation field u. Note that minimizing this energy, $\mathrm{argmin}_u\{E\}$, yields the maximum a posteriori (MAP) estimate of a piece-wise smooth image model affected by Gaussian additive noise. This inverse problem is ill-posed [2, 14]. In order to account for deformation field regularity and to render the problem well-posed, we include limiting and regularization terms into the energy functional [24, 32]:

$$E(u) = \sum_{\forall R} \{ \int_{\Omega_R} (f - \mu_R)^T \Sigma_R^{-1} (f - \mu_R) dx \}$$
$$+ \alpha \int \|u\|^2 dx + \beta \int \left(\|\nabla u_x\|^2 + \|\nabla u_y\|^2 + \|\nabla u_z\|^2 \right) dx \qquad (5)$$

These regularity terms ensure that the segmenting contours in DWI space are still close to their native shape. The model easily allows to incorporate inhomogeneous and anisotropic regularization [25] to better regularize the EPI distortion.

At each iteration, we update the distortion along the steepest energy descent. This gradient descent step can be efficiently tackled by discretizing the time in a forward Euler scheme, and making the right hand side semi-implicit in the regularization terms:

$$\frac{u^{t+1} - u^t}{\tau} = - \sum_{i=1}^{N_c} \left[e(f(c_i')) \hat{n}_{c_i'} \Psi_{c_i}(x) \right] - \alpha u^{t+1} + \beta \Delta u^{t+1} \qquad (6)$$

where the data terms remain functions of the current estimate u^t, thus $c_i' = c_i'(u^t)$. For simplicity on notation, we restricted the number of priors to only 1. We also defined

$e(f(c_i')) = E_{out}(f(c_i')) - E_{in}(f(c_i'))$, and $E_R(f) = (f - \mu_R)^T \Sigma_R^{-1}(f - \mu_R)$. We applied a spectral approach to solve this implicit scheme:

$$u^{t+1} = \mathcal{F}^{-1}\left\{ \frac{\mathcal{F}\left\{u^t/\tau - \sum_{i=1}^{N_c}\left[e(f(c_i'))\hat{n}_{c_i'}\Psi_{c_i}(x)\right]\right\}}{\mathcal{F}\left\{(1/\tau + \alpha)I - \beta\Delta\right\}} \right\} \tag{7}$$

3 Data and experiments

3.1 Shape prior

As described in section 1, the general situation in the connectivity pipelines consists of having a reliable segmentation obtained from the high resolution T1 reference image. Therefore, a precise location of the tissue interfaces of interest is available in a reference space. Given that the anatomical reference segmentation is beyond the scope of this manuscript, we simply rely on the true contours known from the underlying models, and do not seek to establish them in a separate segmentation step on "anatomical" images.

3.2 Synthetic gray-scale data

The first simplified model to test the approach is inspired by a problem shown for coupled CSF/GM and GM/WM segmentation in [23]. Authors note that "partial volume effects blur the distinction between closely adjacent surfaces in deep sulci, leading to a well-known segmentation error in which the deeper reaches of sulci are not penetrated by the putative surface model." This problem is aggravated in DWI, since the resolution tends to be worse compared to the anatomical images considered in [23]. They test their coupled segmentation algorithm on an image, "representing a sulcus in which the distinction between opposing banks of the sulcus has been obscured by partial volume."

Here, we reproduce their model on a volume consisting of three piecewise-constant parts: a notched ball representing the WM with a single sulcus ($\mu_{WM} = 0.8$), a cortical sheet of GM obtained through dilation of the WM ($\mu_{GM} = 0.5$), and the surrounding background representing CSF ($\mu_{CSF} = 0.2$). The volume is then affected by additive Gaussian noise, effectively creating uniform standard deviation of $\sigma = 0.045$ per region.

As illustrated in Figure 1, conventional single surface segmentation of the CSF/GM boundary misses to capture the sulcus in its full depth. With our proposed model, we expect the joint segmentation-registration to be driven largely by the inner, GM/WM contour that exhibits sufficient contrast and lesser partial volume effects. The shape prior of the outer, difficult contour will then be co-aligned through the regularity of the estimated deformation field.

3.3 Simulated diffusion data

In order to demonstrate the functionality of the methodology, and characterize its possibilities with diffusion data, we simulated the DW signal of a synthetic phantom from a model consisting of several spherical shapes emulating the different brain tissues (see Figure 3, first row). We reconstructed the signal with standard procedures to approximate the environment to the real one at maximum.
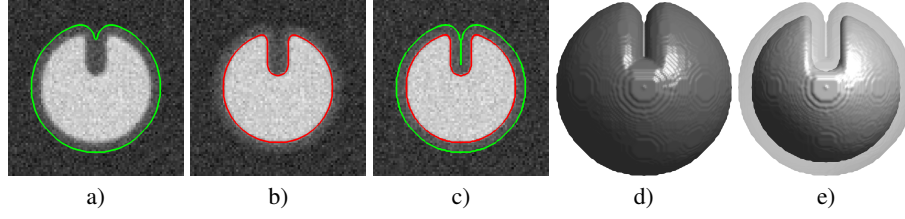
Figure 1. The gray-scale sulcus model. a) The apparent CSF/GM boundary is affected by partial volume in the sulcal cavity, and conventional segmentation is likely to miss it. b) The GM/WM interface here has consistently good contrast. c) Registering the two shape priors coupled through deformation field regularity is expected to guide the CSF/GM contour. d&e) 3D view of the two shape priors.

Signal simulation To numerically simulate the MRI signal attenuation when applying a diffusion gradient in a voxel with N fiber populations we made use of the standard *Multi-Tensor Model* [33]:

$$S(q)/S_0 = \sum_{i=1}^{N} f_i \exp\left(-b\,q^T \mathbf{D}_i\, q\right) + f_{iso} \exp\left(-b\mathbf{D}_{iso}\right), \tag{8}$$

where $q \in \mathbb{S}^2$ is the direction of the diffusion gradient applied, b is the b-value accounting for its strength, $S_0 \equiv S(0)$ is the signal with no diffusion weighting, f_i and $\mathbf{D}_i$ are respectively the volume fraction and the diffusion tensor characterizing the i-th fiber population.

The diffusion tensors $\mathbf{D}_i$ and $\mathbf{D}_{iso}$ describe the diffusion processes of each fiber compartment and of contaminations from the CSF. In this work, these quantities have been taken from standard ranges typically observed in the human brain [4].

Noise simulation The diffusion MRI signal S has been corrupted with *Rician noise* [13] as follows:

$$\tilde{S} = \sqrt{(S+\varepsilon_1)^2 + \varepsilon_2^2} \tag{9}$$

where $\varepsilon_{1,2}$ are Gaussian distributed with zero mean and standard deviation $\sigma = S_0/SNR$ and SNR is the signal-to-noise ratio (SNR) on the S_0 image.

Derived scalar features The target DWI data is characterized by its distortions and its low resolution (typically around $2.2x2.2x3mm^3$). Depending on the posterior reconstruction methodology and the angular resolution intended, the DWI raw data has to be processed in order to extract the information in a manageable manner. The properties of the reconstructed tensors and derived scalar maps have been studied by [9]. Based on their findings, the proposed energy model adapts to the FA (10) and MD (11) for their properties. Whereas FA describes the *shape* of diffusion, the MD depicts the *magnitude* of the process.

$$FA = \sqrt{\frac{1}{2}} \frac{\sqrt{(\lambda_1 - \lambda_2)^2 + (\lambda_2 - \lambda_3)^2 + (\lambda_3 - \lambda_1)^2}}{\sqrt{\lambda_1^2 + \lambda_2^2 + \lambda_3^2}} \tag{10}$$

$$MD = (\lambda_1 + \lambda_2 + \lambda_3)/3 \tag{11}$$

where λ_i are the eigenvalues of the diffusion tensor associated with the diffusion signal $S(q)$. There exist two main reasons to justify their choice. First, they are well-understood and standardized in clinical routine. Second, together they contain most of the information that is usually extracted from the DWI-derived scalar maps.

Simulated distortions For this model, we created manually a sound distortion visually similar to real EPI distortions. We interpolated the distortion to a dense deformation field, necessary for warping the raw DWI simulated data. Once the signal was deformed, we proceeded to reconstruct the diffusion tensor imaging (DTI) and subsequently obtained the scalars of interest (FA, MD). Finally, we estimated their parameters using the tissue probability distribution maps from the original model (Table 1).

Table 1. Model means and covariances of fractional anisotropy and mean diffusivity estimated from the reconstructed simulated DWI images for each modeled tissue, white matter,grey matter, and cerebrospinal fluid. As expected, the two scalar features are complementary and the three tissues can well be discriminated.

Tissue	μ		Σ
	FA	MD	
WM	0.778	6.94×10^{-4}	$\begin{pmatrix} 4.85 \times 10^{-3} & -6.90 \times 10^{-6} \\ -6.90 \times 10^{-6} & 1.03 \times 10^{-8} \end{pmatrix}$
GM	0.119	8.95×10^{-4}	$\begin{pmatrix} 5.90 \times 10^{-4} & -1.43 \times 10^{-6} \\ -1.43 \times 10^{-6} & 1.04 \times 10^{-8} \end{pmatrix}$
CSF	0.103	2.99×10^{-3}	$\begin{pmatrix} 1.19 \times 10^{-3} & 2.22 \times 10^{-7} \\ 2.22 \times 10^{-7} & 1.56 \times 10^{-8} \end{pmatrix}$

4 Results and discussion

4.1 Synthetic gray-scale data

The proposed method solved precisely the specific challenge created by the model. A severe distortion of the model is artificially created adding complexity to the problem of partial voluming in the outer contour of the sulcus. Figure 2 provides visual assessment for this result. With 16x16x16 control points, computation time for this model was around 10 minutes in a (specific machine details).
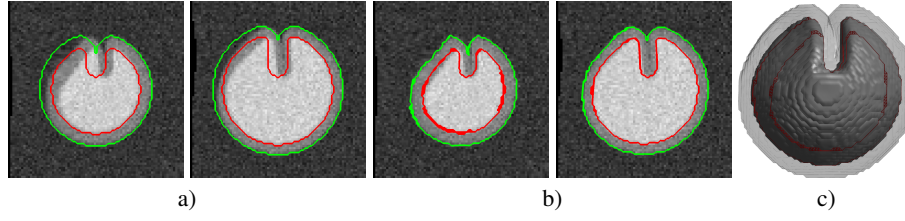
Figure 2. Result of the segmentation performance on the sulcus model. a) Two slices and prior contours before segmentation-registration. b) The same slices and contours after distortion estimation. c) 3D rendering of the deformed priors, with the traces of the two selected slices highlighted. This figure is to be replaced by the real result, this is a proof of concept of registration that does not solve the pv problem. The current figure also removes the outer prior

4.2 Simulated diffusion data

The proposed method successfully reverted the synthetic distortion field we applied to the data. With 16x16x16 control points, the displacements field is dense enough to correctly represent the synthetic field. Second row in Figure 3 shows the fitted contours obtained by using the original surfaces of the model as shape priors, with a constant translation of (5.0mm,10mm.,-5.0mm) to illustrate briefly the extent of the capture range of the algorithm. Computation time in this case was around 4 minutes in the previously described platform.
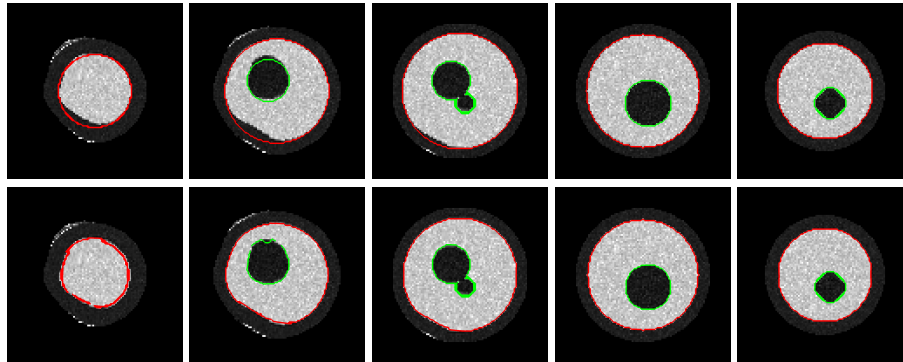

Figure 3. First row presents several slices along Z axis of the distorted FA map and the undistorted WM-GM and WM-CSF contours given as shape priors. Second row contains the same map, now with the contours after joint segmentation-registration.

5 Conclusions and outlook

A novel application for the ACWE framework is proposed, with the aim at recovering the displacement field underlying the EPI geometrical distortions. Exploiting the segmentation properties of the ACWE and optimizing the displacement field, we describe a registration-segmentation methodology that simultaneously segmented and restored the distortion on DWI-like synthetic data. Visual results and quantitative results are provided.

We implemented the methodology upon the widely used Insight Registration and Segmentation Toolkit [5] (ITK) for its computational benefits, the standardized code, and with the aim at making the procedure publicly available when ready for sharing with the research community.

Once proven the aptness of the methodology to the application with simplistic synthetic data, in further studies we will cover the actual performance on real images and the benefits of overcoming the described challenges (segmentation and EPI distortion correction) in one single step.

We conclude stressing on the importance of tackling with the numerous challenges that exist on the DWI data processing in order to achieve reliable results on the whole-brain connectivity analysis.

---

[5] `http://www.itk.org`

Bibliography

[1] Andersson, J.L.R., Hutton, C., Ashburner, J., Turner, R., Friston, K.: Modeling geometric deformations in EPI time series. Neuroimage 13(5), 903–919 (2001)

[2] Bertero, M., Poggio, T.A., Torre, V.: Ill-posed problems in early vision. In: Proceedings of the IEEE. vol. 76, pp. 869–889 (1988)

[3] Bresson, X., Vandergheynst, P., Thiran, J.P.: A Variational Model for Object Segmentation Using Boundary Information and Shape Prior Driven by the Mumford-Shah Functional. International Journal of Computer Vision 68(2), 145–162 (Mar 2006)

[4] Canales-Rodríguez, E., Melie-García, L., Iturria-Medina, Y.: Mathematical description of q-space in spherical coordinates: Exact Q-ball imaging. Magn. Reson. Med. 61(6), 1350–1367 (2009)

[5] Chan, T.F., Vese, L.A.: Active contours without edges. IEEE Transactions on Image Processing 10(2), 266–277 (2001)

[6] Chan, T., Zhu, W.: Level set based shape prior segmentation. In: CVPR 2005. vol. 2, pp. 1164–1170 (2005)

[7] Chen, Y., Tagare, H.D., Thiruvenkadam, S., Huang, F., Wilson, D., Gopinath, K.S., Briggs, R.W., Geiser, E.A.: Using Prior Shapes in Geometric Active Contours in a Variational Framework. International Journal of Computer Vision 50(3), 315–328 (2002)

[8] Cremers, D., Osher, S.J., Soatto, S.: Kernel Density Estimation and Intrinsic Alignment for Shape Priors in Level Set Segmentation. International Journal of Computer Vision 69(3), 335–351 (May 2006)

[9] Ennis, D.B., Kindlmann, G.: Orthogonal tensor invariants and the analysis of diffusion tensor magnetic resonance images. Magnetic Resonance in Medicine 55(1), 136–146 (2006)

[10] Gastaud, M., Barlaud, M., Aubert, G.: Combining Shape Prior and Statistical Features for Active Contour Segmentation. IEEE Transactions on Circuits and Systems for Video Technology 14(5), 726–734 (May 2004)

[11] Gorthi, S., Duay, V., Bresson, X., Bach Cuadra, M., Sánchez Castro, F.J., Pollo, C., Allal, A.S., Thiran, J.P.: Active deformation fields: dense deformation field estimation for atlas-based segmentation using the active contour framework. Medical Image Analysis 15(6), 787–800 (2011)

[12] Gorthi, S., Duay, V., Houhou, N., Bach Cuadra, M., Schick, U., Becker, M., Allal, A.S., Thiran, J.P.: Segmentation of head and neck lymph node regions for radiotherapy planning using active contour-based atlas registration. IEEE Journal of Selected Topics in Signal Processing 3(1), 135–147 (2009)

[13] Gudbjartsson, H., Patz, S.: The Rician distribution of noisy MRI data. Magn. Reson. Med. 34(6), 910–914 (1995)

[14] Hadamard, J.: Sur les problèmes aux dérivées partielles et leur signification physique. Princeton University Bulletin 13, 49–52 (1902)

[15] Hagmann, P.: From diffusion MRI to brain connectomics. Ph.D. thesis, EPFL (2005)

[16] Hagmann, P., Grant, P.E., Fair, D.A.: MR connectomics: a conceptual framework for studying the developing brain. Frontiers in Systems Neuroscience 6 (Jun 2012)

[17] Heiervang, E., Behrens, T., Mackay, C., Robson, M., Johansen-Berg, H.: Between session reproducibility and between subject variability of diffusion MR and tractography measures. NeuroImage 33(3), 867–877 (Nov 2006)

[18] Holland, D., Kuperman, J.M., Dale, A.M.: Efficient correction of inhomogeneous static magnetic field-induced distortion in echo planar imaging. Neuroimage 50(1), 175–183 (Mar 2010)

[19] Hsu, Y.C., Hsu, C.H., Tseng, W.Y.: Correction for susceptibility-induced distortion in echo-planar imaging using field maps and model-based point spread function. IEEE Transactions on Medical Imaging 28(11), 1850–1857 (Nov 2009)

[20] Jezzard, P., Barnett, A.S., Pierpaoli, C.: Characterization of and correction for eddy current artifacts in echo planar diffusion imaging. Magnetic resonance in medicine 39(5), 801–812 (2005)

[21] Johansen-Berg, H., Rushworth, M.F.: Using diffusion imaging to study human connectional anatomy. Annual Review of Neuroscience 32(1), 75–94 (2009)

[22] Jones, D.K., Knösche, T.R., Turner, R.: White matter integrity, fiber count, and other fallacies: The do's and don'ts of diffusion MRI. NeuroImage (Jul 2012)

[23] MacDonald, D., Kabani, N., Avis, D., Evans, A.C.: Automated 3-d extraction of inner and outer surfaces of cerebral cortex from MRI. NeuroImage 12(3), 340–356 (2000)

[24] Morozov, V.A.: Linear and nonlinear ill-posed problems. Journal of Mathematical Sciences II(6), 706–736 (1975)

[25] Nagel, H.H., Enkelmann, W.: An investigation of smoothness constraints for the estimation of displacement vector fields from image sequences. IEEE Transactions on Pattern Analysis and Machine Intelligence 8(5), 565–593 (Sep 1986)

[26] Paragios, N.: A level set approach for shape-driven segmentation and tracking of the left ventricle. IEEE Transactions on Medical Imaging 22(6), 773–776 (Jun 2003)

[27] Pohl, K.M., Fisher, J., Grimson, W.E.L., Kikinis, R., Wells, W.M.: A Bayesian model for joint segmentation and registration. NeuroImage 31(1), 228–39 (May 2006)

[28] Pohl, K.M., Fisher, J., Levitt, J.J., Shenton, M.E., Kikinis, R., Grimson, W.E.L., Wells, W.M.: A Unifying Approach to Registration, Segmentation, and Intensity Correction. In: Duncan, J.S., Gerig, G. (eds.) MICCAI 2005. Lecture Notes in Computer Science, vol. 3749, pp. 310–318. Springer Berlin Heidelberg, Berlin, Heidelberg (2005)

[29] Reber, P.J., Wong, E.C., Buxton, R.B., Frank, L.R.: Correction of off resonance-related distortion in echo-planar imaging using EPI-based field maps. Magnetic Resonance in Medicine 39(2), 328–330 (2005)

[30] Sporns, O., Tononi, G., Kötter, R.: The human connectome: A structural description of the human brain. PLoS computational biology 1(4), e42 (Sep 2005)

[31] Sundgren, P.C., Dong, Q., Gómez-Hassan, D., Mukherji, S.K., Maly, P., Welsh, R.: Diffusion tensor imaging of the brain: review of clinical applications. Neuroradiology 46, 339–350 (May 2004)

[32] Tichonov, A.N.: Solution of incorrectly formulated problems and the regularization method. Soviet Mathematics 4, 1035–1038 (1963)

[33] Tuch, D., Reese, T., Wiegell, M., Makris, N., Belliveau, J., Wedeen, V.: High angular resolution diffusion imaging reveals intravoxel white matter fiber heterogeneity. Magn. Reson. Med. 48(4), 577–582 (2002)

[34] Vemuri, B., Chen, Y.: Joint Image Registration and Segmentation. In: Geometric Level Set Methods in Imaging, Vision, and Graphics. pp. 251–269. Springer-Verlag, New York (2003)

[35] Wakana, S., Caprihan, A., Panzenboeck, M.M., Fallon, J.H., Perry, M., Gollub, R.L., Hua, K., Zhang, J., Jiang, H., Dubey, P., Blitz, A., van Zijl, P., Mori, S.: Reproducibility of quantitative tractography methods applied to cerebral white matter. NeuroImage 36(3), 630–644 (Jul 2007)

[36] Wang, F., Vemuri, B.C., Eisenschenk, S.J.: Joint registration and segmentation of neuroanatomic structures from brain MRI. Academic radiology 13(9), 1104–11 (Sep 2006)

[37] Wyatt, P.P., Noble, J.: MAP MRF joint segmentation and registration of medical images. Medical Image Analysis 7(4), 539–552 (Dec 2003)

[38] Yezzi, A., Zöllei, L., Kapur, T.: A variational framework for integrating segmentation and registration through active contours. Medical Image Analysis 7(2), 171–185 (Jun 2003)

[39] Yezzi, A.J., Soatto, S.: Deformotion : Deforming Motion , Shape Average and the Joint Registration and Approximation of Structures in Images. International Journal of Computer Vision 53(2), 153–167 (2003)

[40] Zöllei, L., Stevens, A., Huber, K., Kakunoori, S., Fischl, B.: Improved tractography alignment using combined volumetric and surface registration. NeuroImage 51(1), 206–213 (May 2010)